THE JOURNAL OF BIOLOGICAL CHEMISTRY VOL. 289, NO. 17, pp. 12096–12108, April 25, 2014

Identification and Functional Characterization of a Novel Bacterial Type Asparagine Synthetase A

*A tRNA SYNTHETASE PARALOG FROM LEISHMANIA DONOVANI**

Received for publication, January 30, 2014, and in revised form, February 22, 2014 Published, JBC Papers in Press, March 7, 2014, DOI 10.1074/jbc.M114.554642

Reetika Manhas[‡1], Pankaj Tripathi[‡2], Sameena Khan[§3], Bhavana Sethu Lakshmi[‡3], Shambhu Krishan Lal[‡3], Venkatraman Subramanian Gowri[‡2], Amit Sharma[§4], and Rentala Madhubala[‡5]

From the [‡]School of Life Sciences, Jawaharlal Nehru University, New Delhi 110067, India and [§]Structural and Computational Biology Group, International Centre for Genetic Engineering and Biotechnology, New Delhi 110067, India

Background: Asparagine synthetase A catalyzes the synthesis of asparagine from aspartate in the presence of ammonia as a nitrogen donor.
Results: *L. donovani* ASNA enzyme is of bacterial origin and is both ammonia- and glutamine-dependent.
Conclusion: *Ld*ASNA is essential for survival of the *Leishmania* parasite.
Significance: The absence of *Ld*ASNA homologs from humans validates *Leishmania* ASNA as a novel drug target.

Asparagine is formed by two structurally distinct asparagine synthetases in prokaryotes. One is the ammonia-utilizing asparagine synthetase A (AsnA), and the other is asparagine synthetase B (AsnB) that uses glutamine or ammonia as a nitrogen source. In a previous investigation using sequence-based analysis, we had shown that *Leishmania* spp. possess asparagine-tRNA synthetase paralog asparagine synthetase A (*Ld*ASNA) that is ammonia-dependent. Here, we report the cloning, expression, and kinetic analysis of ASNA from *Leishmania donovani*. Interestingly, *Ld*ASNA was both ammonia- and glutamine-dependent. To study the physiological role of ASNA in *Leishmania*, gene deletion mutations were attempted via targeted gene replacement. Gene deletion of *Ld*ASNA showed a growth delay in mutants. However, chromosomal null mutants of *Ld*ASNA could not be obtained as the double transfectant mutants showed aneuploidy. These data suggest that *Ld*ASNA is essential for survival of the *Leishmania* parasite. *Ld*ASNA enzyme was recalcitrant toward crystallization so we instead crystallized and solved the atomic structure of its close homolog from *Trypanosoma brucei* (*Tb*ASNA) at 2.2 Å. A very significant conservation in active site residues is observed between *Tb*ASNA and *Escherichia coli* AsnA. It is evident that the absence of an *Ld*ASNA homolog from humans and its essentiality for the parasites make *Ld*ASNA a novel drug target.

Leishmania donovani is a protozoan parasite that causes visceral leishmaniasis, a disease that is fatal if left untreated. Visceral leishmaniasis treatment primarily relies on chemotherapy due to problems related to vector control and lack of an effective vaccine to treat the disease (1). Because of the development of resistance against currently available antileishmanial drugs (2, 3), there is a growing need for discovering novel drug targets and developing new inhibitors.

Asparagine synthetase (L-aspartate:ammonia ligase (AMP-forming), EC 6.3.1.1) is an enzyme that catalyzes the synthesis of asparagine from aspartate using adenosine triphosphate (ATP) as the energy source in the presence of a nitrogen donor (4). The nitrogen donor can be glutamine or ammonia. Two families of asparagine synthetases are known to date. One is asparagine synthetase A (AsnA),[6] which utilizes nitrogen only from an ammonia source (4). AsnA family members have been reported from prokaryotes such as *Escherichia coli* and *Klebsiella aerogenes* (5, 6) as well as from archaea such as *Pyrococcus abyssi* (7, 8). The other family is asparagine synthetase B (AsnB) whose members are found in prokaryotes and eukaryotes (9–11). Members of the AsnB family preferentially utilize glutamine as the nitrogen source, although they are capable of utilizing both glutamine and ammonia. *E. coli* and *K. aerogenes* have two asparagine synthetase genes, *asnA* and *asnB*, and the presence of either ensures sufficient asparagine biosynthesis, whereas inactivation of both causes asparagine auxotrophy (12). Although they are eukaryotes, *Leishmania* and *Trypanosoma* surprisingly possess both ASNA (LmjF.26.0830) and ASNB (LmjF.29.1490) (13).

Asparagine is formed in two steps: the β-carboxylate group of aspartate is first activated by ATP to form an aminoacyl-AMP before its amidation by a nucleophilic attack with an ammonium ion. Interestingly, this mechanism of amino acid activation resem-

* This work was supported by a grant from the Department of Biotechnology, Government of India and a Department of Science and Technology Promotion of University Research and Scientific Excellence grant (to R. M.).
The atomic coordinates and structure factors (code 4LNS) have been deposited in the Protein Data Bank (http://wwpdb.org/).
[1] Recipient of funding from the University Grants Commission, India.
[2] Kothari postdoctoral fellows supported by the University Grants Commission, India.
[3] Recipients of funding from the Council of Scientific and Industrial Research, India.
[4] Supported by an Outstanding Scientist Research Programme in Biotechnology grant from the Department of Biotechnology, Government of India and a J. C. Bose National Fellow.
[5] A J. C. Bose National Fellow. To whom correspondence should be addressed. Tel. and Fax: 91-11-26742630; E-mail: rentala@outlook.com.

[6] The abbreviations used are: AsnA, asparagine synthetase A; AsnB, asparagine synthetase B; *Ld*ASNA, *L. donovani* asparagine synthetase A; *Tb*ASNA, *T. brucei* asparagine synthetase A; *ASNA*OE, *ASNA* overexpressor; CMXRos, *chloromethyl-X-rosamine; HYG*, hygromycin phosphotransferase gene; *NEO*, neomycin phosphotransferase gene; *Ec*AsnA, *E. coli* asparagine synthetase A.

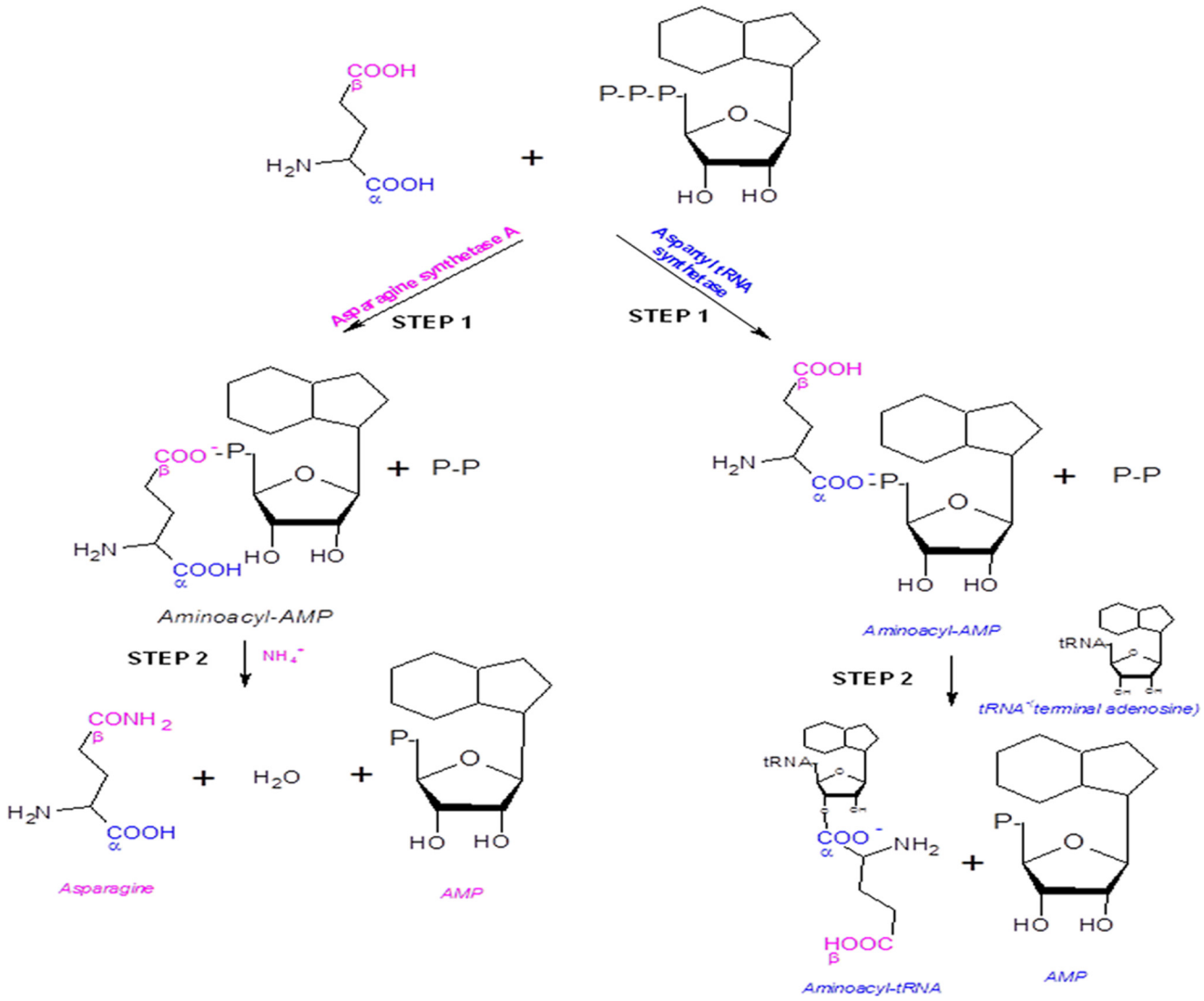

FIGURE 1. **Schematic representation of the reaction mechanisms of asparagine synthetase A and aspartyl-tRNA synthetase enzymes.** *Step 1* involves activation of the selective carboxyl groups by the respective enzymes to form aminoacyl-AMP. *Step 2* involves amidation of the aminoacyl-AMP by asparagine synthetase A and transfer of the activated amino acid to the cognate tRNA by aspartyl-tRNA synthetase.

bles that used by aminoacyl-tRNA synthetases, which first activate the α-carboxylate group of an amino acid to form also an aminoacyl-AMP before they transfer the activated amino acid onto cognate tRNA (Fig. 1) (4). We had previously reported a novel asparagine-tRNA synthetase paralog, asparagine synthetase A from *Leishmania major* (13). These paralogs retain the typical aminoacyl-tRNA synthetase catalytic domain with class II motifs but are devoid of the anticodon binding domain (14). Such paralogs have been reported only from prokaryotes and archaea so far (8, 15) where they participate in amino acid biosynthesis (*e.g.* AsnA and HisZ) and lysylation of a specific lysine in elongation factor P (GenX/PoxA) (8, 14, 16–20).

Asparagine biosynthesis is an unexplored area in kinetoplastids. Despite being eukaryotes, kinetoplastids and other parasites such as *Trichomonas vaginalis*, *Entamoeba histolytica*, and *Cryptosporidium parvum* possess an ammonia-dependent asparagine synthetase (AsnA-type) enzyme (13). Detailed sequence-based phylogenetic analysis reveals a close relationship of these parasitic ASNA enzymes to the ammonia-dependent AsnA-type enzymes of *E. coli* and other bacteria (13). A recent report indicates that asparagine synthetase A-knocked down *T. brucei* were auxotrophic to asparagine (21). To date, crystal structures of AsnA-type enzymes from *E. coli* and *P. abyssi* are known (8, 22). We report, for the first time, identification, molecular cloning, expression, and enzymatic characterization of a eukaryotic ASNA-type enzyme from *Leishmania donovani*. We additionally crystallized and solved the atomic structure of the *L. donovani* ASNA (*Ld*ASNA) homolog from *Trypanosoma brucei* (*Tb*ASNA). *L. donovani* and *T. brucei* share a sequence identity of ~80%; therefore, the crystal structure of *Tb*ASNA provides a platform for structure-function studies on these enzymes. Gene replacement study indicates that the enzyme asparagine synthetase A (ASNA) from *Leishmania donovani* plays an essential role in the viability of this pathogenic organism.

EXPERIMENTAL PROCEDURES

Materials—All restriction enzymes and DNA-modifying enzymes were obtained from MBI Fermentas (Germany). Neo-

mycin, paromomycin, blasticidin, and hygromycin were obtained from Sigma-Aldrich. Plasmid pET-30a was obtained from Novagen. Protein markers and DNA ladders were acquired from New England Biolabs. L-Aspartic acid, L-glutamine, lactate dehydrogenase, myokinase, and pyruvate kinase were obtained from Sigma-Aldrich. Other materials used in this study were of analytical grade and were commercially available.

Leishmania Strains and Culture Conditions—L. donovani Bob (*Ld*Bob strain/MHOM/SD/62/1SCL2D) promastigotes were cultured at 22 °C in M199 medium (Sigma) supplemented with 100 units/ml penicillin (Sigma), 100 μg/ml streptomycin (Sigma), and 5% heat-inactivated fetal bovine serum (Hyclone). Medium was additionally supplemented with 10 μg/ml hemin. Genetically manipulated parasites were derived from wild type *L. donovani* Bob originally obtained from Dr. Stephen Beverley (Washington University, St. Louis, MO). Wild type (WT) parasites were routinely cultured in medium with no drug supplementations, whereas the *ASNA* heterozygotes (*ASNA*/*HYG* and *ASNA*/*NEO*) and *ASNA*/*NEO*/*HYG* parasites were maintained in either 150 μg/ml hygromycin, 300 μg/ml paromomycin, or both, respectively. The *ASNA* overexpressor (*ASNA*OE) parasites were maintained in 10 μg/ml blasticidin. pSP72-α-neo-α-GFP-*ASNA*-transfected parasites were maintained in 40 μg/ml G418. For characterizing the single transfectant, double transfectant, and *ASNA*-overexpressing parasites phenotypically, cells were subcultured without the selection marker prior to experiments.

Construction of Expression Vectors and Purification of the Proteins—A 1062-bp DNA fragment encompassing the whole open reading frame (ORF) of the *LdASNA* gene was amplified from genomic DNA using a sense primer with a flanking BamHI site (5′-CGGGATCCATGTCGTCCAGTCCGCAGGAGTACATT-3′) and an antisense primer with a flanking HindIII site (5′-CCCAAGCTTTTACAATAAGGAGTACTGCGTCGTGACCTC-3′). A single ~1062-bp PCR product was obtained. The amplified product was cloned into BamHI and HindIII restriction sites of pET-30a vector using T4 DNA ligase (New England Biolabs). The fidelity of the PCR amplification of *LdASNA* was confirmed by automated DNA sequencing. Sequence comparison of *ASNA* was done using the NCBI search algorithm BLAST. Multiple amino acid sequence alignment was performed using the program ClustalW with default parameters (23). The *T. brucei* (*Tb*ASNA-pET28a) construct was kindly provided by Dr. Cordeiro da Silva (Institute for Molecular and Cell Biology, University of Porto, Portugal) (21). *Ld*ASNA-pET30a or *Tb*ASNA-pET28a constructs containing a His_6 tag at the N terminus were transformed into *E. coli* BL-21 strain. Expression from the constructs *Ld*ASNA-pET30a or *Tb*ASNA-pET28a was induced at an $A_{600\ nm}$ of 0.6 with 0.1 mM isopropyl 1-β-D-galactopyranoside at 16 °C for 16 h. Bacteria were then harvested by centrifugation at 5000 × *g* for 10 min, and the cell pellet was resuspended in lysis buffer (50 mM Tris-Cl, pH 7.4, 10 mM imidazole, 300 mM sodium chloride, 2 mM phenylmethylsulfonyl fluoride, and protease inhibitor mixture). The resulting cell suspension was sonicated six times for 30 s at 1-min intervals. The lysate was centrifuged at 10,000 × *g* for 30 min at 4 °C. The resulting supernatant, which contained the protein, was loaded onto pre-equilibrated Ni^{2+}-nitrilotriacetic acid-agarose resin (Qiagen). The protein was eluted with increasing concentrations of imidazole. The purified protein was found to be >95% pure as judged by SDS-PAGE.

*Tb*ASNA was used for crystallization studies. The purest fractions were checked by SDS-PAGE and concentrated by using a 10-kDa-cutoff Centricon centrifugal device (Millipore). The protein was further purified by gel filtration chromatography on an S200 analytical gel filtration column (GE Biosciences) in buffer containing 50 mM Tris-Cl, 200 mM NaCl, and 10 mM β-mercaptoethanol, pH 7.5, for apoenzyme crystallization. The final protein was concentrated to ~73 mg/ml (using $A_{280\ nm}$) and stored at −80 °C. The concentration of the purified protein was determined using Bradford reagent (Sigma).

Sequence Identification Decoding Analysis of ASNA Protein by MALDI-TOF—After protein visualization, the ASNA protein band was excised from SDS-PAGE gel and subjected to matrix-assisted laser desorption/ionization time of flight mass spectrometry (MALDI-TOF/TOF). The MALDI-TOF mass spectra were recorded with an Autoflex II mass spectrometer (Bruker Daltonics, Germany) installed in the Advanced Instrumentation Facility, Jawaharlal Nehru University (New Delhi, India). The obtained spectra were calibrated externally with software available with the instrument. Initial sequences were subjected to flexControl and BioTools. Final sequence identification and scoring was performed using the Mascot search tool.

*Asparagine Synthetase Assay—Ld*ASNA-catalyzed asparagine synthesis activity was measured in a coupled enzyme system at 37 °C using a Varian Cary® 100 UV-visible spectrophotometer. The formed product (AMP) was coupled to an adenylate kinase, pyruvate kinase, and lactate dehydrogenase reaction for oxidation of NADH to NAD. The resultant decrease of NADH was monitored at 340 nm (4). The reaction mixture (1.0 ml) contained 100 mM Tris-HCl, pH 7.8, 1.5 mM L-aspartic acid, 20 mM NH_4Cl, 3 mM ATP, 100 mM KCl, 10 mM $(CH_3COO)_2Mg$, 1 mM phosphoenolpyruvate, 0.24 mM of NADH, 5 mM DTT, 2 units of myokinase, 10 units of pyruvate kinase, and 25 units of lactate dehydrogenase. Kinetic analysis was done using 20 μg of the enzyme. Progress of the reaction was scanned against a buffer blank for 1200 s with an interval of 30 s at a wavelength of 340 nm. Determination of the K_m and V_{max} for L-aspartate, ATP, and NH_4^+ was achieved by varying the concentration of each component in the reaction mixture while maintaining others in excess. To confirm substrate specificity of the enzyme, L-glutamine was used as a nitrogen source instead of NH_4Cl. The *Ld*ASNA activity in cell lysates of WT Bob, *ASNA*OE, and heterozygous (*ASNA*/*HYG* and *ASNA*/*NEO*) parasites was determined as reported above. Cell lysates of all the strains were prepared by repeated freeze/thaw. Statistical analyses were undertaken using GraphPad Prism 5.0 (GraphPad Software, Inc.).

Cloning of the pSP-α-blast-α-ASNA and pSP72-α-neo-α-GFP-ASNA Episome—For overexpression of *ASNA* gene in *L. donovani*, the 1062-bp *ASNA* ORF was amplified by PCR using the forward primer 5′-TTTTTCTAGAATGTCGTCCAGTCCGCAGGAGTACATT-3′ with a flanking XbaI site (underlined) and the reverse primer 5′CCCAAGCTTTTACAATAAGGAGTACTGCGTCGTGACCTC-3′ with a flanking

TABLE 1
Primers used for generation of the hygromycin (Hyg)- and neomycin (Neo)-specific linear replacement cassette fragments

L. donovani primers	Sequences
A	5′-ACAGCGAACGAAATCGAGCG-3′
B_{Hyg}	5′-GGTGAGTTCAGGCTTTTTCATGGCTGGCAGTGAAAGAAAAAGGGATGAATGGA-3′
C_{Hyg}	5′-TCCATTCATCCCTTTTTTCTTTCACTGCCAGCCATGAAAAAGCCTGAACTCAC-3′
D_{Hyg}	5′-GTTCCACCACCCTCCCCCGTCTTTCTATTCCTTTGCCCTCGGACGAG-3′
E_{Hyg}	5′-CTCGTCCGAGGGCAAAGGAATAGAAAGACGGGGGAGGGTGGGTGGGAACGCCT-3′
B_{Neo}	5′-AATCCATCTTGTTCAATCATGGCTGGCAGTGAAAGAAAAAGGGATGAATGGA-3′
C_{Neo}	5′-TCCATTCATCCCTTTTTTCTTTCACTGCCAGCCATGATTGAACAAGATGGATT-3′
D_{Neo}	5′-GTTCCACCACCCTCCCCCGTCTTTTCAGAAGAACTCGTCAAGAAG-3′
E_{Neo}	5′-CTTCTGACGAGTTCTTCTGAAAAGACGGGGGAGGGTGGGTGGGAACGCCT-3′
F	5′-AGGCGTCGCTCCGCTCTGCACTTTC-3′

HindIII site (underlined). The amplified DNA fragment *LdASNA* was cloned into the XbaI-HindIII site of pSP-α-blast-α vector (*Leishmania*-specific vector) containing a blasticidin acetyltransferase gene as the selection marker as reported earlier (24). The *LdASNA*-GFP construct was made by cloning *LdASNA* in pSP72-α-neo-α-GFP vector at BamHI and XbaI sites. The forward primer 5′-TTTGGATCCATGTCGTCCAGTCCGCAGGAGTACATT-3′ (BamHI site underlined) and the reverse primer 5′-TTTTTCTAGACAATAAAGAGTACTGCGCCGTGACCTC-3′ (XbaI site underlined) were used for amplification. Correct orientation and sequence fidelity of the inserts were verified by nucleotide sequence analysis.

Localization of ASNA in L. donovani—pSP72-α-neo-α-GFP-*ASNA*-transfected promastigotes were used for studying the localization of ASNA in *L. donovani*. Fluorescence imaging of stabilized culture was performed using a confocal laser scanning microscope (Zeiss LSM 510 META) equipped with a 63× objective at an excitation wavelength of 488 nm. Briefly, 10^6 promastigotes/ml were pelleted and resuspended in phosphate-buffered saline (PBS) containing 1% fetal bovine serum (FBS) with identical final cell concentration. Cells were pelleted and resuspended in 500 μl of ice-cold 4% paraformaldehyde and incubated on ice for 20 min. Promastigotes were then washed with PBS before treating them with 0.5% Triton X-100 in PBS for 5 min at room temperature. DAPI (0.5 μg/ml) (Invitrogen) was added and washed with PBS before microscopy. Parasites stained with DAPI were observed at an excitation wavelength of 405 nm. Furthermore, to investigate possible mitochondrial localization, 10^7 promastigotes/ml were pelleted and stained with MitoTracker Red-CMXRos (1 nM) (Molecular Probes, Eugene, OR) in fresh medium for 10–15 min to locate mitochondria. The cells were then washed twice with PBS containing 1% FBS and resuspended in the same PBS solution with identical final cell concentration. Promastigotes were then immobilized on poly-L-lysine-coated glass slides. For observing fluorescence of parasites stained with MitoTracker Red-CMXRos, the parasites were visualized using a confocal laser scanning microscope at an excitation wavelength of 568 nm.

Molecular Constructs for the Replacement of the ASNA Alleles—A targeted gene replacement strategy was used for inactivation of *ASNA* gene in *L. donovani*. A fusion PCR-based strategy was used as reported earlier (25). Briefly, *ASNA*-flanking regions were amplified from *L. donovani* wild type genomic DNA and ligated to hygromycin phosphotransferase gene (*HYG*) or neomycin phosphotransferase gene (*NEO*). The 5′-UTR (1000 bp) of *L. donovani ASNA* was obtained by PCR amplification with primers A and B_{Hyg} or primers A and B_{Neo} (Table 1). The *NEO* gene was amplified from pX63-NEO with primers C_{Neo} and D_{Neo}. The *HYG* gene was amplified from pX63-HYG with primers C_{Hyg} and D_{Hyg} (Table 1). The 3′-UTR (750 bp) of *L. donovani ASNA* was obtained from *L. donovani* wild type genomic DNA by PCR amplification using primer E_{Hyg} and reverse primer F or with primer E_{Neo} and reverse primer F (Table 1). The 5′-UTR of *L. donovani ASNA* was then ligated to the antibiotic resistance marker gene by PCR using primers A and D_{Hyg} or A and D_{Neo}. This fragment (5′-UTR-marker gene) was fused with 3′-UTR of *ASNA* using primers A and F, yielding the fragment 5′-UTR-Hyg-3′-UTR or 5′-UTR-Neo-3′-UTR.

TABLE 2
Primers used for the molecular characterization of the genetically manipulated parasites by PCR-based analysis

L. donovani primers	Sequences
Primer 1	5′-TGTAGAAGTACTCGCCGATAGTGG-3′
Primer 2	5′-CGACACAATACTCTGGCGCTGGAGC-3′
Primer 3	5′-CGCAGCTATTTACCCGCAGGACAT-3′
Primer 4	5′-ATGACGGAGGCCCTCTCCTTTTTGC-3′
Primer 5	5′-ATAGCGTTGGCTACCCGTGATATTGC-3′
Primer 6	5′-AACACGGCGGCATCAGAGCAGCCGATTG-3′
Primer 7	5′-CGAGGTCACGGCGCAGTACTCTTTA-3′
Primer 8	5′-GGTCTGGAGATCAATGTACTCCTGC-3′

Generation of Genetically Manipulated Parasites—After PCR amplification and purification, ~2–3 μg of linear replacement cassette fragment 5′-UTR-Hyg-3′-UTR or 5′-UTR-Neo-3′-UTR were individually transfected by electroporation in wild type *L. donovani* promastigotes (26). Depending on the marker gene, transfectants were selected in the presence of 150 μg/ml hygromycin (Sigma) or 300 μg/ml paromomycin (Sigma). After three to four passages, cells resistant to antibiotic selection were subjected to PCR-based analysis to check for the correct integration of the replacement cassettes using primers shown in Table 2. Thereafter, a second round of transfection was initiated to knock out the other copy of *ASNA* gene. The replacement cassette fragment 5′-UTR-Hyg-3′-UTR was used to transfect *ASNA*/*NEO* heterozygous parasites, and 5′-UTR-Neo-3′-UTR was used to transfect *ASNA*/*HYG* heterozygous parasites to generate homozygous *ASNA* gene deletion mutants. A similar PCR-based analysis was carried out to check for the correct integration of the replacement cassettes as was done in the case of *ASNA* heterozygotes. Furthermore, the genotypes of the *ASNA* mutants were confirmed by Southern analysis using standard protocols (27).

The *L. donovani* strain overexpressing ASNA was made by transfecting wild type *L. donovani* promastigotes with the pSP-α-blast-α-*ASNA* construct. The transfected cells were main-

tained in 10 μg/ml blasticidin. Wild type *L. donovani* transfected with pSP-α-blast-α vector was used for comparison. 20 μg of pSP72-α-neo-α-GFP-*ASNA* plasmid was transfected into the wild type *L. donovani* promastigotes for localization studies. The transfected cells were maintained in 40 μg/ml G418. A control transfection with vector alone was used for comparison.

Growth Studies—Growth rate experiments were conducted by inoculating stationary phase parasites at a density of 1×10^6 cells/ml in M199 medium with 5% FBS in 25-cm^2 flasks without respective selection drug and culturing at 22 °C. Growth rates of each of the cultures were determined at 24-h intervals by using a Neubauer hemocytometer. Growth studies with each individual cell line were done at least three times, and similar results were obtained each time.

Crystallization, Data Collection, and Structure Determination—*Tb*ASNA crystals (apo form) were obtained at 20 °C by the hanging drop vapor diffusion method using 1 μl of *Tb*ASNA and 1 μl of 10% (w/v) PEG 20000, 20% (v/v) PEG monomethyl ether 550, 0.03 M NPS (sodium nitrate, disodium hydrogen phosphate, ammonium sulfate), and 0.1 M MOPS/HEPES-Na, pH 7.5. A plate-shaped single crystal was directly mounted in cooled nitrogen gas at 100 K. X-ray diffraction data were collected on a MAR CCD x-ray detector at BM14 beam line of the European Synchrotron Radiation Facility at Grenoble, France. A total of 360 images were collected with 12-s exposure each and 0.5° oscillations per frame. The diffraction images were processed and scaled with HKL2000 (28). The initial model was built by AutoBuild in PHENIX (29), which was subsequently rebuilt manually using Coot (30). Model refinement was performed using phenix.refine in PHENIX. Structural superimposition and figures were generated using Chimera (31). Coordinates and structure factors for *Tb*ASNA have been deposited in the RCSB Protein Data Bank under accession code 4LNS.

Statistical Analysis—Data are represented as mean ± S.D. A value of $p < 0.05$ was accepted as an indication of statistical significance. Results for enzyme activity in the cell lysates were entered as column data in GraphPad Prism 5.0 (GraphPad Software, Inc.) and analyzed by Student's *t* test.

RESULTS

Sequence Analysis and Genomic Organization—ASNA sequences have been identified in each of the *Leishmania infantum* and *L. major* genomes (see the European Molecular Biology Laboratory-European Bioinformatics Institute web site). ASNA sequences have also been identified in the *T. brucei* 927 (*Tb*927.7.1110) and *Trypanosoma cruzi* Es genomes (*Tc*00.1047053503899.90). In addition to kinetoplastids, BLAST searches against EuPathDB (32) suggest that parasites such as *T. vaginalis* (A2EKG5), *E. histolytica* (C4LT17), and *C. parvum* (Q5CPD9) possess a copy of *ASNA* gene. BLAST analysis of *L. major* and *L. infantum* genomes revealed that the ASNA-encoding gene is present on chromosome 26. *Trypanosoma* and *Leishmania* contain a single copy of *ASNA* gene (33). Sequence analysis, database search, and alignment of the *Ld*ASNA amino acid sequence were performed. The *Ld*ASNA amino acid sequence had a single open reading frame consisting of 1062 bp. The ORF encoded a putative polypeptide of 353 amino acids with a predicted molecular mass of 40 kDa. Sequence analysis suggests that asparagine synthetase A enzymes from kinetoplastids share reasonably high sequence identity (~60%). *E. coli* AsnA is 58% identical to *Ld*ASNA and 60% identical to *Tb*ASNA. *Lactobacillus delbrueckii* and *E. histolytica* share sequence identity of ~45% with *Ld*ASNA and *Tb*ASNA. Archaeal sequences are distant homologs with low (<15%) identity to *Ld*ASNA and *Tb*ASNA sequences. Phylogenetic analysis reveals a close relationship of kinetoplastid enzymes to *E. coli* and other bacterial ammonia-dependent AsnA-type enzymes (13).

Cloning, Overexpression, and Purification of LdASNA—*Ld*ASNA is predicted to be of ~40-kDa molecular mass with a theoretical pI of 5.4 using the ExPASy bioinformatics tool ProtParam. To characterize the recombinant *Ld*ASNA protein, the full-length gene was cloned into the backbone fragment of pET-30a expression vector. The resultant construct pET30a-*Ld*ASNA with an N-terminal His_6 tag and thrombin protease cleavage site was transformed into *E. coli* (BL21). A single band of homogenously purified *Ld*ASNA protein with an N-terminal His_6 tag was identified with a molecular mass of ~44 kDa (Fig. 2*A*). Purification yielded ~3 mg of purified protein/liter of bacterial culture. To further characterize *Ld*ASNA, the purified protein was analyzed by MALDI-TOF/TOF mass spectroscopy (Fig. 2*B*). The spectrum of the protein analyzed by BioTools version 2.2 showed an intensity coverage of 35.8% for putative asparagine synthetase A (*L. infantum* JPCM5). The polypeptide sequence fragments covered in the MS/MS data for each peak are colored *red* in Fig. 2*B*. A sequence search analysis by a Mascot search revealed top scores of 99 and 74 with putative asparagine synthetase A of *Leishmania* spp. with accession numbers gi|146089599 and gi|398016957, respectively. These results confirm the presence of a putative asparagine synthetase A in *L. donovani*.

Enzymatic Activity and Kinetic Parameters for LdASNA—Asparagine synthetase A catalyzes the synthesis of asparagine, AMP, and PP_i in the presence of ATP, L-aspartate, and NH_4^+ (4). To determine any ammonium-dependent asparagine synthesis activity of *Ld*ASNA, the product AMP was coupled with an NADH oxidation reaction (4). In the case of prokaryotic organisms, ammonium- and glutamine-dependent asparagine synthesis activity, each corresponding to a nitrogen source of NH_4^+ or glutamine, respectively, has been reported (10, 15). In archaea bacteria, *e.g. P. abyssi*, asparagine formation occurs only by the process of amidation of aspartate (34). To establish the kinetic parameters and specificity of *Ld*ASNA using L-aspartate, ATP, and N_2 source, we examined the effect of various concentrations of substrate L-aspartate while other components were kept constant (Fig. 3*A*). The V_{max} value for L-aspartate was determined to be 69.6 ± 2 nmol min^{-1} mg of $protein^{-1}$. The K_m value of *Ld*ASNA for L-aspartate was measured to be 0.6 ± 0.08 mM, which is closer to that reported in the case of *K. aerogenes* (0.91 mM) (6). ATP is an essential component for substrate amidation during the asparagine synthesis reaction. Therefore, we performed ATP-dependent enzyme kinetic studies (Fig. 3*B*). In the case of *Ld*ASNA, the estimated V_{max} value was 63.5 ± 1.3 nmol min^{-1} mg of $protein^{-1}$, and the K_m for ATP was 1.2 ±

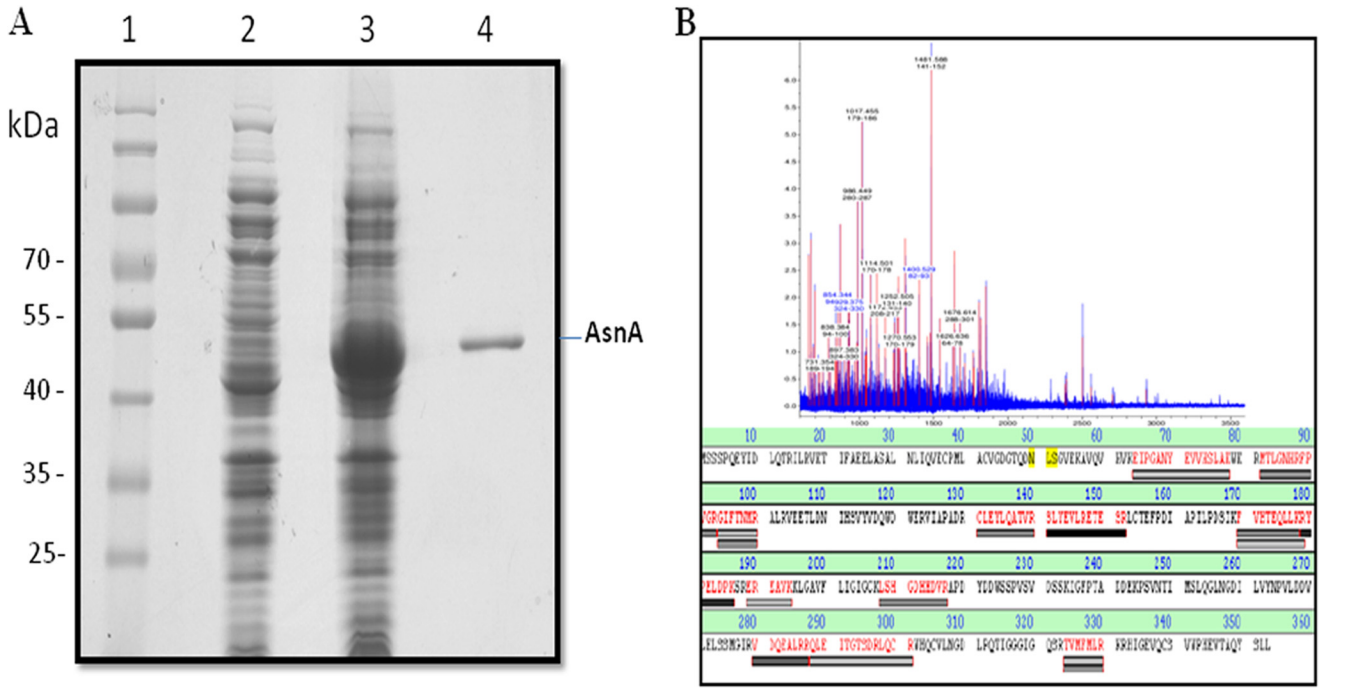

FIGURE 2. *A*, purification of recombinant *Ld*ASNA protein on Ni^{2+}-nitrilotriacetic acid affinity resin. *Lane 1*, molecular mass marker; *lane 2*, uninduced cell lysate; *lane 3*, induced cell lysate; *lane 4*, eluted fraction with 200 mM imidazole showing purified *Ld*ASNA. *B*, MALDI-TOF peptide mass fingerprinting and alignment of the identified peptides of a tryptic digest of *Ld*ASNA protein obtained after nickel-nitrilotriacetic acid purification.

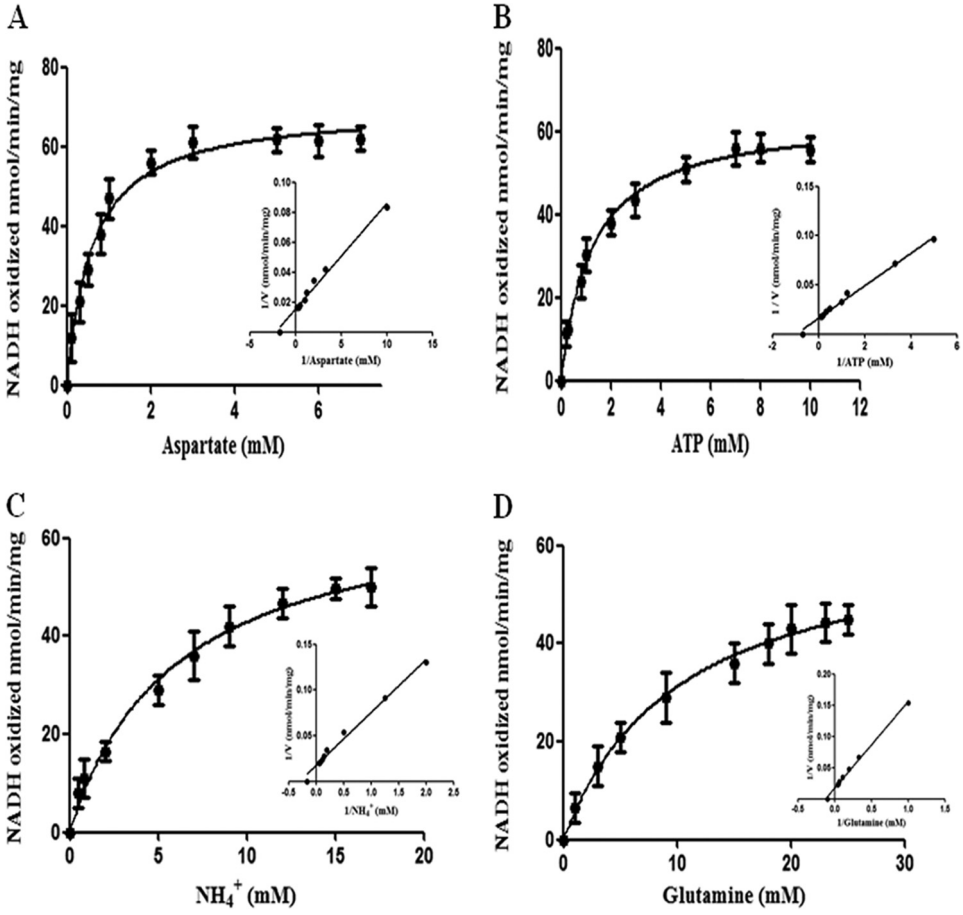

FIGURE 3. **Michaelis-Menten and Lineweaver-Burk plots (*inset*) for conversion of L-aspartic acid to asparagine by *Ld*ASNA enzyme.** The enzyme assay was carried out as described under "Experimental Procedures." *A–D*, kinetic constants were computed using the Michaelis-Menten algorithm within GraphPad Prism 5.0 for utilization of L-aspartate, ATP, NH_4Cl, and L-glutamine by *Ld*ASNA enzyme. Results are representative data from three separate experiments and are represented as mean ± S.E. (*error bars*).

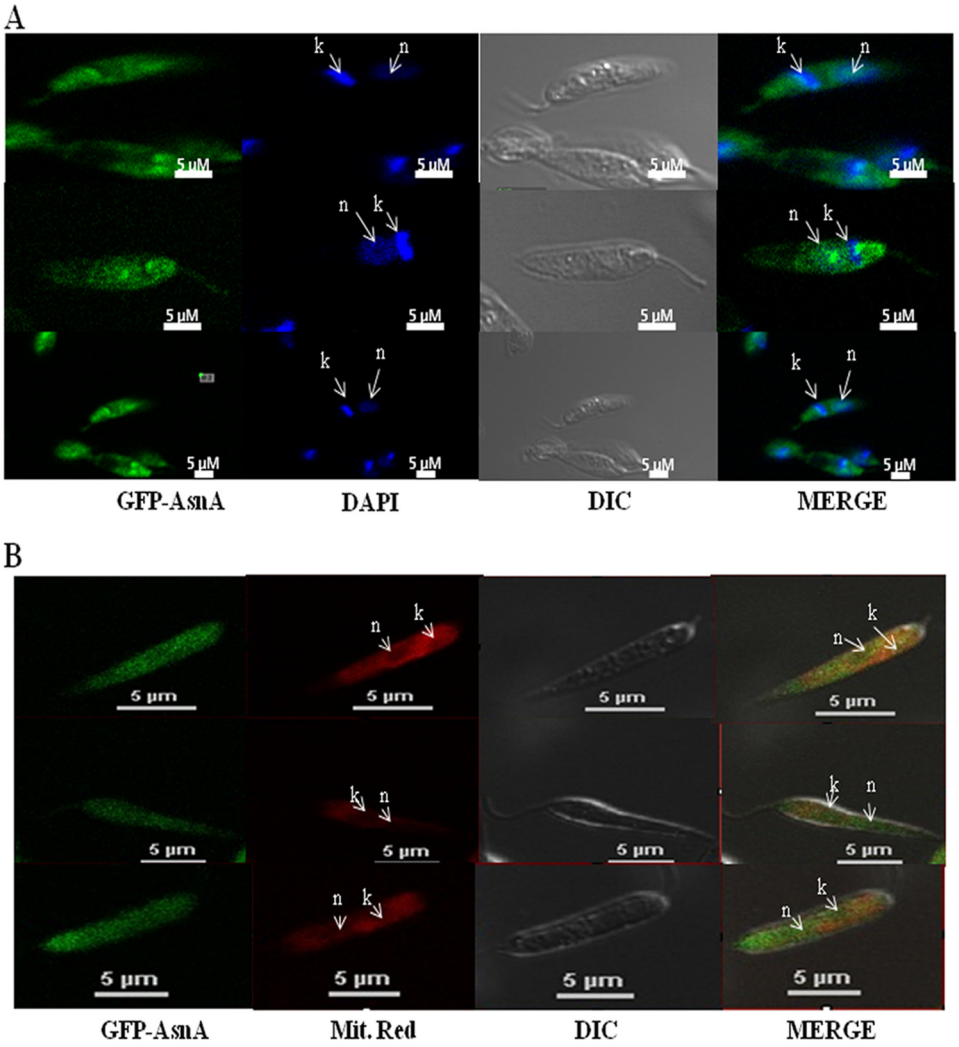

FIGURE 4. *A*, confocal microscopy of wild type *L. donovani* transfected with pSP72-α-neo-α-GFP-*ASNA*. *First panel*, wild type *L. donovani* expressing *Ld*ASNA as a GFP translational fusion protein; *second panel*, wild type *L. donovani* stained with DAPI; *third panel*, phase-contrast image; *fourth panel*, merged micrograph. *B*, co-localization of *Ld*ASNA in mitochondria. *First panel*, wild type *L. donovani* expressing *Ld*ASNA as a GFP translational fusion protein; *second panel*, wild type *L. donovani* stained with MitoTracker Red; *third panel*, phase-contrast image; *fourth panel*, merged micrograph. "*k*" and "*n*" indicate kinetoplastid and nuclear DNA, respectively. Results are representative data from three separate experiments. *DIC*, differential interference contrast.

0.09 mM. To establish the N_2 source specificity, we measured *Ld*ASNA activity with various concentrations of NH_4^+ and L-glutamine (Fig. 3, *C* and *D*). An *Ld*ASNA V_{max} value of 68.4 ± 3.6 nmol min^{-1} mg of $protein^{-1}$ and K_m value of 5.95 ± 0.8 mM was obtained for NH_4^+, which is closer to that reported for *Streptococcus bovis* (4.0 mM) and *T. brucei* (5.55 mM) (21, 35). Interestingly, *Ld*ASNA was found to be capable of utilizing L-glutamine as the nitrogen source. This feature never reported before appears to be unique for kinetoplastid ASNAs as has also been recently reported in case of *T. brucei* and *T. cruzi* (21). The kinetic parameters obtained for the utilization of L-glutamine for *Ld*ASNA were a V_{max} value of 63.4 ± 1.8 nmol min^{-1} mg of $protein^{-1}$ and K_m value of 10.3 ± 0.7 mM. Hence, we conclude that *Ld*ASNA is active and preferentially utilizes ammonia, although it is also capable of utilizing glutamine as a nitrogen source (Fig. 3, *C* and *D*).

Subcellular Localization of LdASNA—The GFP-*Ld*ASNA construct was designed for episomal expression in *L. donovani* parasites as described under "Experimental Procedures." This construct was electrotransformed in parasites and selected as reported earlier (36). *L. donovani* parasites transfected with the GFP-*Ld*ASNA fusion constructs were fixed and analyzed by fluorescence microscopy. GFP fluorescence was detectable in ~60% of the cells transfected with the fusion constructs. The kinetoplast and nuclear DNA in these cells were readily identified by their bright staining with DAPI (Fig. 4*A*). GFP-*Ld*ASNA was found to be present in the cytoplasm of the parasite (Fig. 4*A*). We repeated localization studies several times and viewed ~90 different parasites. The parasites transfected with the GFP vector alone (lacking an insert) showed GFP fluorescence in the entire promastigote (data not shown). *L. major* ASNA appears to have predicted mitochondrial (PSORT II) and cytosolic (MARSPred) localization. However, the mitochondrion-targeting signal peptide sequences and the cleavage sites could not be predicted by any of the currently available computational tools. Therefore, we wanted to probe mitochondrial localization of *Ld*ASNA, so GFP-*Ld*ASNA construct-transfected parasites were stained with MitoTracker Red (Fig. 4*B*). Our data indicate localization of ASNA in both the cytosol and mitochondria of the parasites.

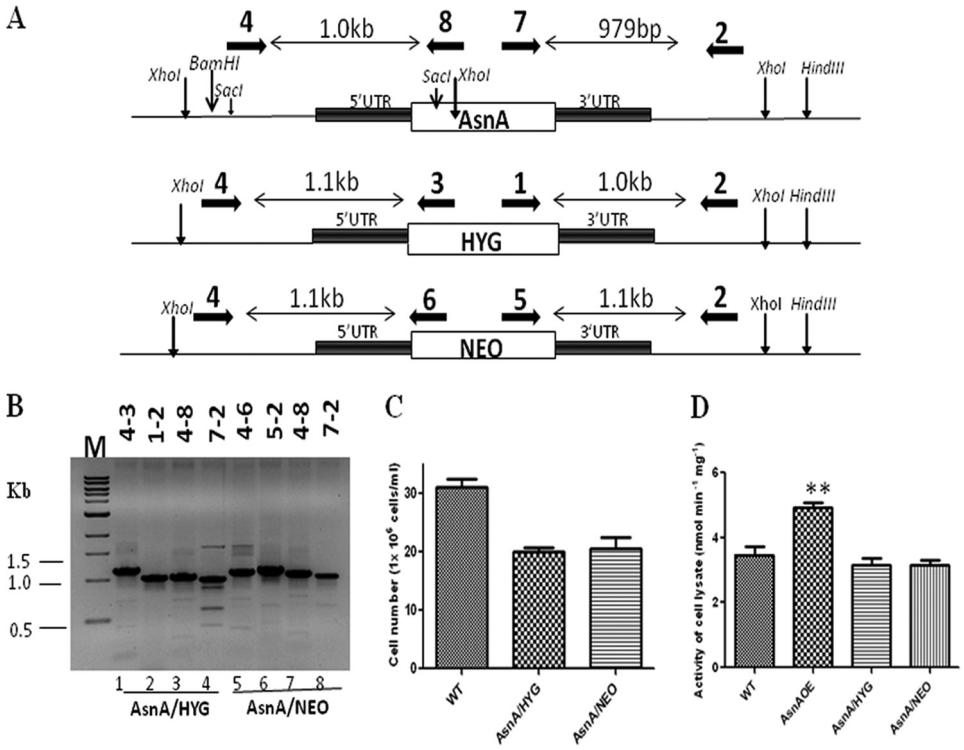

FIGURE 5. *A*, restriction map of the *LdASNA* genomic locus and the location of the primers used for confirmation by PCR analysis along with the expected band sizes. Primer 4 was designed as a forward primer to match the upstream region of *LdASNA* gene, and primers 8, 3, and 6 were designed to be internal to *ASNA*, *HYG*, and *NEO* coding regions, respectively. Primer 2 was designed as a reverse primer to match the downstream region of *LdASNA* gene, and primers 7, 1, and 5 were designed as forward primers internal to *ASNA*, *HYG*, and *NEO* coding regions, respectively. *B*, genomic DNA from *ASNA*/*HYG* and *ASNA*/*NEO* heterozygous parasites was used as a template for PCR analysis. The specific integration of the replacement cassette was checked with *LdASNA*- and *HYG*- or *NEO*-specific primers. *M* indicates the molecular size marker in kb. *C*, growth analysis of *L. donovani* WT and single transfectants *ASNA*/*HYG* and *ASNA*/*NEO*. The parasites were counted after 4 days on a hemocytometer. These results represent mean ± S.D. (*error bars*) with $n = 3$. *D*, comparison of the *Ld*ASNA enzyme activity (nmol min^{-1} mg^{-1}) of WT Bob, *ASNA*OE, *ASNA*/*HYG*, and *ASNA*/*NEO* in the respective cell lysates by an NADH-ATP coupled reaction. These results represent mean ± S.D. (*error bars*) with $n = 3$. **, $p < 0.01$.

Gene Deletion Studies of Asparagine Synthetase A—The essentiality of *LdASNA* was assessed by classical gene replacement experiments where attempts were made to replace both copies of *LdASNA* by drug resistance genes. Cassettes having *HYG* or *NEO* as selection markers along with the flanking 5′-UTR and 3′-UTR of *LdASNA* gene were used to replace *LdASNA* as described under "Experimental Procedures" (Fig. 5*A*). Linear replacement cassettes made by fusion PCR were electrotransfected into wild type *L. donovani* promastigotes, leading to generation of heterozygous parasites in which one copy of *LdASNA* gene was replaced with either the hygromycin or neomycin drug resistance gene. Replacement of a single copy of *LdASNA* gene from the chromosome by the hygromycin or neomycin drug resistance gene cassette was confirmed by PCR-based analysis by using primers external to the inactivation cassette of *LdASNA* gene (Fig. 5*A*). Cells transfected with the replacement cassette were selected after three to four passages. DNA from the transfected *L. donovani* promastigotes was isolated and subjected to PCR-based analysis. 1.1- and 1.0-kb bands in the case of the *HYG* cassette and 1.1- and 1.1-kb bands in the case of the *NEO* cassette along with the 1.0-kb and 979-bp bands corresponding to the WT *LdASNA* gene were also obtained (Fig. 5*B*). This confirmed that a single copy of *LdASNA* gene had been replaced in heterozygotes parasites. Interestingly, the heterozygous parasites consistently showed a growth delay compared with wild type parasites (Fig. 5*C*). The ASNA activity was lower in heterozygous parasites in comparison with the wild type strain (Fig. 5*D*). It is reasonable to assume that a gene dosage effect resulted in the production of lesser ASNA protein, and such a conjecture would suggest that ASNA is involved in optimal cell proliferation.

*Ld*ASNA heterozygotes were subsequently transfected with a second cassette to replace the second copy of the gene. PCR analysis demonstrated that cells selected on the double antibiotic medium showed *HYG* and *NEO* replacement cassettes at the *LdASNA* gene locus similar to the heterozygotes, but these transfectants also showed 1.0-kb and 979-bp bands corresponding to the WT *LdASNA* gene (data not shown). This result indicates the presence of wild type gene in the double transfectants.

The presence of WT *LdASNA* gene along with *HYG* and *NEO* replacement cassettes in the *LdASNA* gene locus was further checked by Southern blot analysis by digesting the genomic DNA with XhoI. In the WT cells, digestion of *WT LdASNA* gene locus with XhoI was expected to yield a 2.7-kb band after probing with the 5′-UTR of *LdASNA* gene as probe (Fig. 6*A*). Integration of the *HYG* or *NEO* cassette in single transfectants was expected to yield 5- and 4.8-kb 5′-UTR-hybridizing bands, respectively, in addition to the 2.7-kb wild type band (Fig. 6*A*). Bands of the expected sizes hybridizing with the *L. donovani ASNA* 5′-UTR as probe were obtained in the case of the heterozygous parasites (Fig. 6*B*), but in the case of double trans-

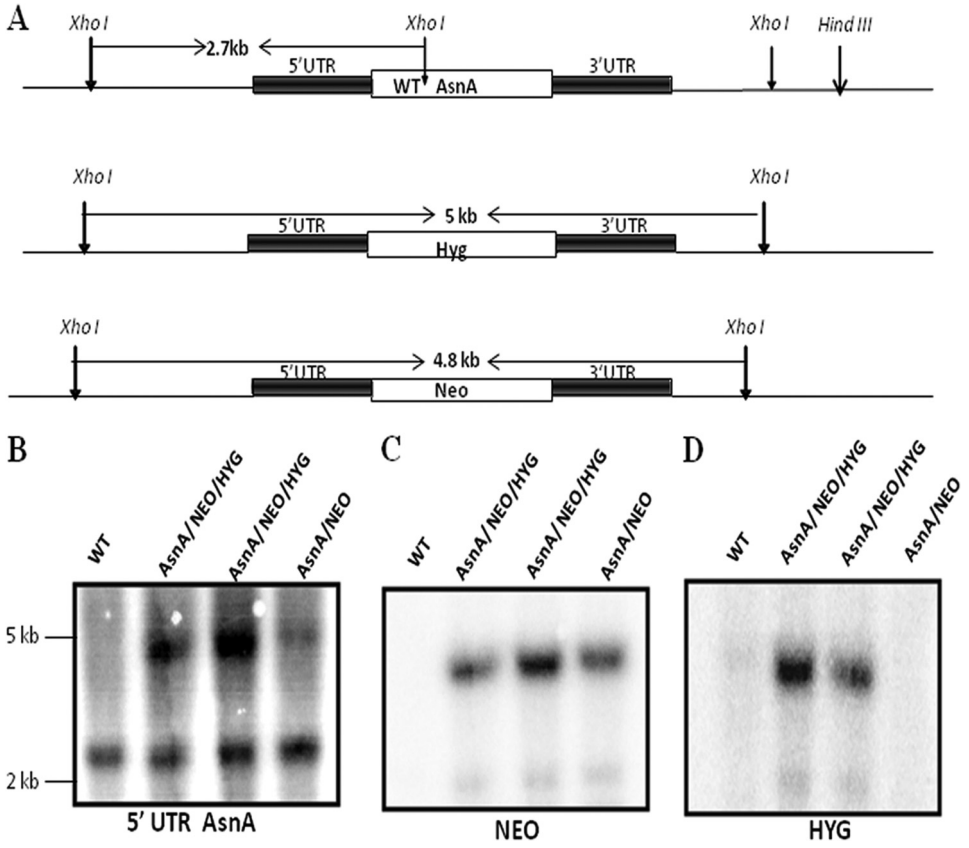

FIGURE 6. *A*, restriction map of the *LdASNA* locus and the predicted chromosomal rearrangements occurring during *HYG* and *NEO* replacement of *ASNA* in the chromosomal locus. *B*, Southern blot analysis of WT Bob, single transfectant *ASNA*/*NEO*, and double transfectant *ASNA*/*NEO*/*HYG*. Genomic DNA was digested with XhoI, separated on a 0.6% agarose gel, and probed with the 5′-UTR of *LdASNA*. Molecular size markers are indicated to the *right* of the blot. *C* and *D*, blot in *B* was striped and reprobed with the *NEO* or *HYG* gene, respectively, to indicate the presence of *NEO* and *HYG* in single and double transfectants.

fectants, a band corresponding to the WT *LdASNA* was found, indicating the presence of WT gene in these transfectants. The same blot probed with the *HYG* and *NEO* genes as probes showed the presence of both *HYG* and *NEO* in double transfectants (Fig. 6, *C* and *D*). At least five clones of each of the transfectant cell lines were picked and screened for phenotypic characterization. All attempts to generate *Ld*ASNA homozygous null mutant were unsuccessful. Southern blot analyses demonstrated that the *LdASNA* gene was still present in the genome of these parasite lines, indicating that *LdASNA* may be an essential gene.

Because the double transfectant mutant clones (*ASNA*/*HYG*/*NEO*) were found to contain 2.7-kb wild type *ASNA* allele as well as *HYG* and *NEO* integrations, DNA content-based analysis was performed to check the ploidy levels of the cells. Fluorescence-activated cell sorting (FACS) analysis of fixed cells stained with propidium iodide was performed to determine the ploidy levels of WT and single and double transfectants. In the wild type cells, two peaks corresponding to 2N (G_1) and 4N (G_2) DNA content were observed as expected. An identical pattern was observed with the heterozygous mutants *ASNA*/*HYG* and *ASNA*/*NEO*, thus indicating that these heterozygous parasites contain normal diploid DNA content similar to wild type cells. Interestingly, FACS analysis of the double transfected parasite clone (*ASNA*/*HYG*/*NEO*) showed peaks that corresponded to 3N and 6N DNA content (data not shown). This suggests a difference in the ploidy level in the cell population of the double transfectant parasites when compared with the single transfectants and wild type cells. The G_1 and G_2 peaks of the double transfected parasite indicated that these cells are aneuploid (data not shown). All the single and double transfected clones screened showed similar results.

Crystal Structure Analysis—The *Tb*ASNA crystal structure was solved by molecular replacement using *Ec*AsnA (Protein Data Bank code 11AS) as the search model in apo form. The structure was refined using native diffraction data at 2.2-Å resolution. *Tb*ASNA crystals belong to space group ($P6_122$) with one monomer of *Tb*ASNA in the asymmetric unit. *Tb*ASNA exists as a homodimer inside the crystals (based on packing considerations) (Table 3). The final electron density for the *Tb*ASNA model is well defined except for loop 1 (residues 51–57) and loop 2 (residues 210–250; Figs. 7–9). The structure of *Tb*ASNA (monomer) consists of 10 β-strands and 10 α-helices (Fig. 7). Sequence identity between *Leishmania* and the *E. coli* enzyme counterpart is ~57%, and the overall fold of *Tb*ASNA is hence very similar to that of *Ec*AsnA. *Tb*ASNA and *Ec*AsnA monomers superimpose with a root mean square deviation of ~1.2 Å for 304 C^{α} atoms. However, residues 210–250 in *Tb*ASNA have a unique ~19-residue insertion (in the *Tb*ASNA sequence, this insertion is QVVFPRTSKPIPTMNSLSS; in *Ld*ASNA, it is KIGFPTADDEKPSVNTIMS) as part of loop 2 (Fig. 8). The significance of this insertion at this location in the structure of *Tb*ASNA is unclear because in the crystal structure of apo-*Tb*ASNA this loop is completely disordered. Further-

more, these ~19-residue insertions seem to have little sequence conservation between *Tb*ASNA and *Ld*ASNA. In contrast, a structure-based multiple sequence alignment between *T. brucei* and *L. donovani* ASNA shows very few regions of sequence divergence (Fig. 7). Therefore, the role of insertion sequences in ASNAs may need to be explored sepa-

TABLE 3

Data collection and refinement statistics

Values in parentheses are for the highest resolution shell. r.m.s.d., root mean square deviation.

Data collection	
Wavelength (Å)	0.976
Crystal-to-detector distance (mm)	232.1
Exposure time (s)	12
Number of frames	360
Unit cell parameters (Å; °)	$a = 71.55$, $b = 71.55$, $c = 268.63$; $\alpha = 90$, $\beta = 90$, $\gamma = 120$
Space group	$P6_122$
Resolution (Å)	25.0-2.20 (2.24-2.20)
Unique reflections	21721 (1082)
Multiplicity	8.0 (8.5)
Completeness (%)	99.6 (100)
$I/\sigma(I)$	27.14 (3.2)
R_{merge}	0.076 (0.482)
Refinement	
Resolution (Å)	24.6-2.20
Reflections in work set/test set	20,543/1,105
R_{work}/R_{free} (%)	20.5/25.0
Stereochemistry	
r.m.s.d. in bond lengths (Å)	0.008
r.m.s.d. in bond angles (°)	1.17
Ramachandran plot	
Residues in most favored regions (%)	93.7
Residues in additionally allowed regions (%)	6.3

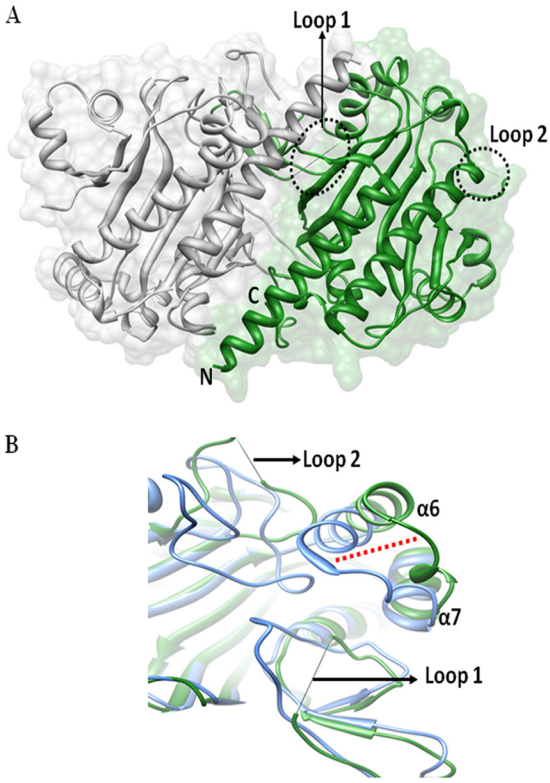

FIGURE 8. *A*, overall structure of *Tb*ASNA in apo form. The monomers that form ASNA dimer are shown with loop 1 and loop 2 highlighted in *black dots*. Loops 1 and 2 are disordered in *Tb*ASNA, although in the *E. coli* apoenzyme, they are ordered. *B*, superposition of *Tb*ASNA and *Ec*AsnA monomer showing α-helices 6 and 7 that are displaced from their *Ec*AsnA counterparts by ~9 Å.

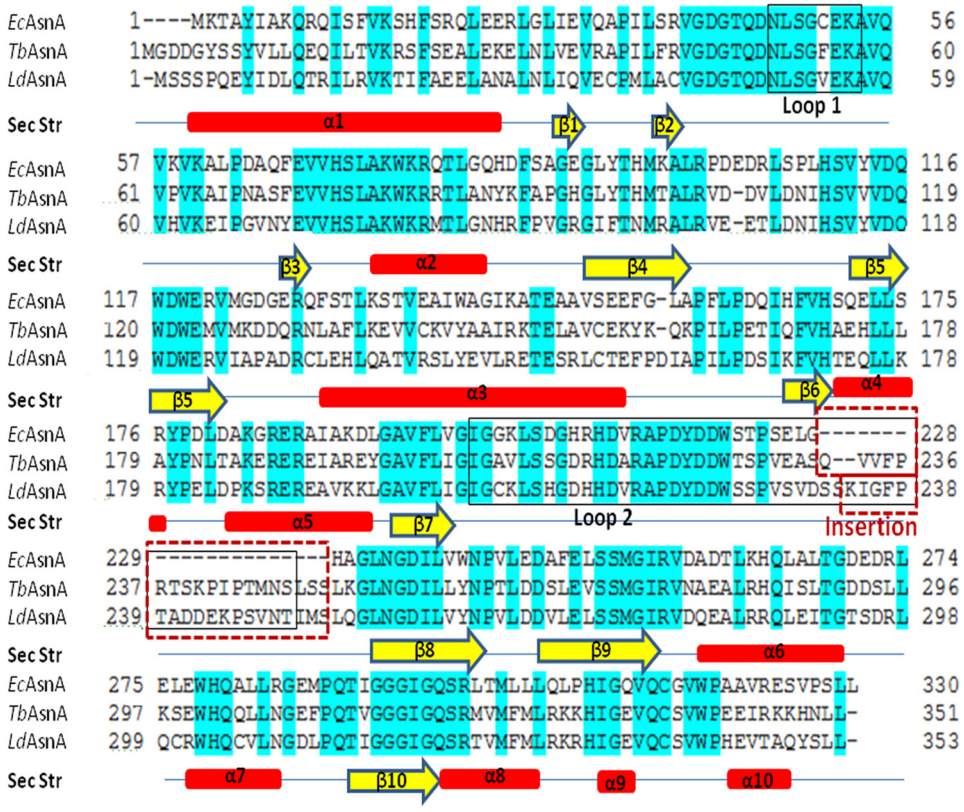

FIGURE 7. **Sequence alignment of *Tb*ASNA and *Ld*ASNA with *Ec*AsnA.** The secondary structure (*Sec Str*) elements derived from the crystal structure of *Tb*ASNA are placed at the *bottom* of the alignment. The loop in *Tb*ASNA and *Ld*ASNA (herein called loop 2) contains a ~19-residue insertion (*red box*) that is absent in *E. coli* and archaeal AsnAs.

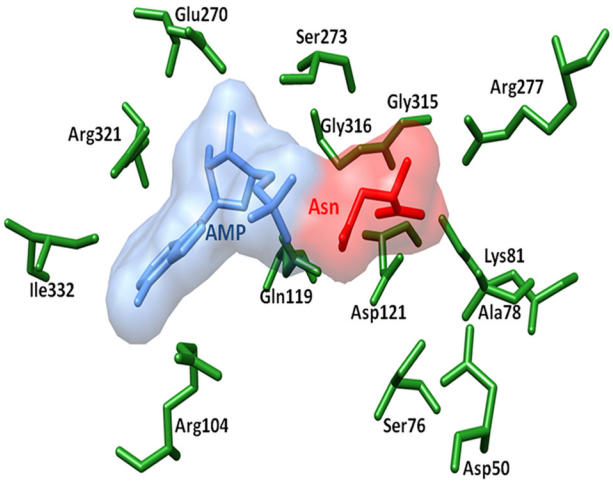

FIGURE 9. **Superposition of *Ec*AsnA complexed with Asn and AMP and *Tb*ASNA.** Ligands are shown as space-filling models. L-Asn (*red*), AMP (*blue*), and side chains of *Tb*ASNA are shown (*green*). The corresponding *Ec*AsnA side chains have been removed for simplicity. All the L-Asn- and AMP-binding side chains are conserved between *E. coli* and *Tb*ASNA and *Ld*ASNA.

rately. From the structure of *Tb*ASNA, it is evident that α-helices 6 and 7 are distinctly displaced from their *E. coli* AsnA counterparts by up to ~9 Å. Furthermore, in *Ec*AsnA, there are no major conformational changes between the apo and holo forms of the enzyme. Indeed, the apo form of *Tb*ASNA shows no significant deviation from its *E. coli* counterpart except in the noted ~9-Å displacement near α-helices 6 and 7 (Fig. 8*B*). Using visualization software (Chimera), we cataloged active site amino acid residues (a total of 15) that interact with L-Asn and AMP in the crystal structure of *Ec*AsnA (Protein Data Bank code 12AS). We then mapped these L-Asn- and AMP-binding active site residues onto the *Tb*ASNA structure (Fig. 9). Interestingly, all 15 active site residues (of which seven recognize L-Asn and eight bind AMP) are conserved among *E. coli*, *Tb*ASNA, and *Ld*ASNA. Residue Tyr-218 in *Ec*AsnA is part of loop 2, and although it remains conserved, it is disordered in *Tb*ASNA. These constraints within the active sites of ASNAs, therefore, can be exploited to screen specific inhibitors that can selectively target these enzymes. The high resolution atomic structure presented here can serve as a platform for development of specific inhibitors against both *Tb*ASNA and *Leishmania* ASNA.

DISCUSSION

Aminoacyl-tRNA synthetase paralogs involved in amino acid biosynthesis have been known for many years (8, 14, 16–19). These activities include AsnA (asparagine-tRNA synthetase paralog), HisZ (histidyl-tRNA synthetase paralog), and lysylation of a specific lysine in bacterial *elongation factor P* (GenX/PoxA). Among these, *E. coli* AsnA and GenX/PoxA are well characterized (8, 14, 16–20, 22). Because they are absent in humans but present in pathogenic organisms like *Leishmania*, these paralogs form a novel category of drug targets. Our earlier detailed bioinformatics analysis revealed the presence of ASNA paralogs in certain eukaryotic pathogens (13, 37). Recently, characterization of ASNA from *T. brucei* and *T. cruzi* has been reported (21). Although the asparagine-tRNA synthetases contain a synthetase domain and an anticodon binding domain, these paralogs contain only the synthetase domain to perform asparagine biosynthesis (13). We had reported earlier that although aminoacyl-tRNA synthetases of *L. major* are suggested to be of archaeal/eukaryotic origins, *L. major* asparagine synthetase A is likely to be of bacterial origin (13).

Two structurally distinct groups of asparagine synthetases are known in prokaryotes: the ammonia-utilizing asparagine synthetases (AsnA) and glutamine-utilizing asparagine synthetases (AsnB). Although *asnB* genes are reported from all three domains of life, *asnA* genes have been reported from prokaryotes (15), archaea (8), and very recently eukaryotic pathogens (13, 21, 37). AsnA is present in certain anaerobic Gram-positive bacteria such as *Clostridium perfringens*, *Bacillus anthracis*, *Streptococcus pneumoniae*, and *Clostridium botulinum.* AsnA also exists in certain facultative anaerobic Gram-negative bacteria such as *E. coli*, *Yersinia enterocolitica*, *Salmonella enterica*, *Yersinia pestis*, and *Shigella flexneri* (33). *Enterocytozoon bieneusi* is the only fungal pathogen that has an *ASNA* gene (33). It is also the only eukaryotic pathogen with 45 copies of *ASNA* genes of variable amino acid lengths ranging from 50 to 300 amino acids long (33). Interestingly, ASNA is present only in *C. parvum* and *Cryptosporidium hominis* and is absent from other apicomplexan parasites (33). Among Viridiplantae, a single copy of *ASNA* gene is present in *Thalassiosira pseudonana* CCMP 1335 (33). *T. vaginalis* is the other eukaryotic pathogen that carries a copy of *ASNA* gene (13).

In this study, we show that *Ld*ASNA is an ammonia-dependent AsnA-type enzyme also capable of utilizing glutamine as the nitrogen source. The overall K_m values deduced by kinetic analysis for *Ld*ASNA appear to be closer to those reported earlier in the case of prokaryotic organisms (6, 35) Attempts to delete the *ASNA* gene from the parasite genome failed, and these parasites showed aneuploidy. Thus, *L. donovani ASNA* appears to be an essential gene. However, *ASNA* knockdown in *T. brucei* did not affect *in vitro* growth of bloodstream forms of the parasite (21).

Previous crystal structure analysis of *Ec*AsnA suggested a class II catalytic core of aminoacyl-tRNA synthetases for these enzymes (22). Structure-based sequence comparison of *Ec*AsnA with the catalytic domain of yeast aspartyl-tRNA synthetase showed a high conservation of catalytic residues (22). Although the substrates of these two enzymes are similar, the activation of carboxyl groups on the aspartyl residues is different. Yeast aspartyl-tRNA synthetase activates the α-carboxyl group of the substrate, whereas *Ec*AsnA activates the β-carboxyl group (22). The recent crystal structure of an archaeal AsnA from *P. abyssi* in various substrate-bound forms helped to decode the plausible mechanism of asparagine biosynthesis by AsnA in archaea (8). Sequence-based phylogenetic analysis of the *Ld*ASNA followed by structural modeling and comparison with the *E. coli* AsnA suggested an evolutionary origin of kinetoplastid *ASNA* genes closer to that of the prokaryotic AsnA rather than the archaeal enzyme (13). The *Ld*ASNA is also expected to follow a similar catalytic mechanism as *Ec*AsnA based on its structural similarity to archaeal AsnA (13). Our extensive attempts to crystallize recombinant *Ld*ASNA failed, but we were able to solve the high resolution crystal structure of the highly homologous *Tb*ASNA. Sequence iden-

tity between *Ld*ASNA and *Tb*ASNA is ~80%. As expected, the overall fold of *Tb*ASNA is similar to that of *Ec*AsnA, and their respective monomers superimpose with a root mean square deviation of ~1.2 Å for 304 C^{α} atoms (Figs. 7–9). The loop in *Tb*ASNA and *Ld*ASNA (herein called loop 2) contains a unique 19-residue insertion of variable sequence that is absent from *E. coli* and archaeal AsnAs. In both the apo and holo structures of *Ec*AsnA, loop 2 is ordered, suggesting that ligand engagement is not necessary for ordering of loop 2. However, in the *Tb*ASNA structure of the apoenzyme, the corresponding loop 2 with its unique 19-residue insertion remains fully disordered. We also observed very high sequence conservation in 15 residues that line the active site pockets of these enzymes (Fig. 9). Hence, the presented crystal structure of *Tb*ASNA can serve as a model for structure-based inhibitor design against not only *Ld*ASNA but, given the extensive active site conservation (residues that interact with L-Asn and AMP are identical) noted previously, possibly also for other homologs of ASNA from various pathogens that harbor this enzyme.

Asparagine synthetase is a potential target for cancer chemotherapy (38) because asparagine depletion caused by the administration of L-asparaginase is presently being used as a protocol for the treatment of acute lymphoblastic leukemia (39). Therefore, it is highly desirable to develop inhibitors of ASNA that could be used as chemotherapeutic agents. Koizumi *et al.* (40) synthesized a transition state analog of cysteine sulfoximine, *N*-adenylated *S*-methyl-L-cysteine sulfoximine. This inhibitor was found to be an extremely potent slow binding inhibitor of *E. coli* AsnA. This inhibitor was also found to inhibit AsnB effectively and irreversibly (41). The crystal structure of *E. coli* asparagine synthetase A in complex with its potent slow binding inhibitor has revealed the structural basis for transition state stabilization as well as for substrate recognition (40). Our analyses of ASNA from *Leishmania* parasites along with the structure of its homolog from *Trypanosoma* together provide a rationale for targeting this enzyme in drug discovery efforts. The absence of ASNA from humans and its essentiality in *Leishmania* together provide a new window for exploiting ASNA for drug development to treat visceral leishmaniasis.

Acknowledgments—We thank the Advance Instrumentation Research Facility at Jawaharlal Nehru University for providing the imaging facility and for MALDI-TOF analysis. We also thank Marc Ouellette, University of Laval, Quebec, Canada for providing Leishmania shuttle vectors.

REFERENCES

1. Freitas-Junior, L. H., Chatelain, E., Kim, H. A., and Siqueira-Neto, J. L. (2012) Visceral leishmaniasis treatment: what do we have, what do we need and how to deliver it? *Int. J. Parasitol. Drugs Drug Resist.* **2,** 11–19
2. Maltezou, H. C. (2010) Drug resistance in visceral leishmaniasis. *J. Biomed. Biotechnol.* **2010,** 617521
3. García-Hernández, R., Manzano, J. I., Castanys, S., and Gamarro, F. (2012) *Leishmania donovani* develops resistance to drug combinations. *PLoS Negl. Trop. Dis.* **6,** e1974
4. Sugiyama, A., Kato, H., Nishioka, T., and Oda, J. (1992) Overexpression and purification of asparagine synthetase from *Escherichia coli*. *Biosci. Biotechnol. Biochem.* **56,** 376–379
5. Humbert, R., and Simoni, R. D. (1980) Genetic and biomedical studies demonstrating a second gene coding for asparagine synthetase in *Escherichia coli*. *J. Bacteriol.* **142,** 212–220
6. Reitzer, L. J., and Magasanik, B. (1982) Asparagine synthetases of *Klebsiella aerogenes*: properties and regulation of synthesis. *J. Bacteriol.* **151,** 1299–1313
7. Charron, C., Roy, H., Blaise, M., Giegé, R., and Kern, D. (2004) Crystallization and preliminary x-ray diffraction data of an archaeal asparagine synthetase related to asparaginyl-tRNA synthetase. *Acta Crystallogr. D Biol. Crystallogr.* **60,** 767–769
8. Blaise, M., Fréchin, M., Oliéric, V., Charron, C., Sauter, C., Lorber, B., Roy, H., and Kern, D. (2011) Crystal structure of the archaeal asparagine synthetase: interrelation with aspartyl-tRNA and asparaginyl-tRNA synthetases. *J. Mol. Biol.* **412,** 437–452
9. Hughes, C. A., Beard, H. S., and Matthews, B. F. (1997) Molecular cloning and expression of two cDNAs encoding asparagine synthetase in soybean. *Plant Mol. Biol.* **33,** 301–311
10. Scofield, M. A., Lewis, W. S., and Schuster, S. M. (1990) Nucleotide sequence of *Escherichia coli asnB* and deduced amino acid sequence of asparagine synthetase B. *J. Biol. Chem.* **265,** 12895–12902
11. Van Heeke, G., and Schuster, S. M. (1989) Expression of human asparagine synthetase in *Escherichia coli*. *J. Biol. Chem.* **264,** 5503–5509
12. Yoshida, K., Fujita, Y., and Ehrlich, S. D. (1999) Three asparagine synthetase genes of *Bacillus subtilis*. *J. Bacteriol.* **181,** 6081–6091
13. Gowri, V. S., Ghosh, I., Sharma, A., and Madhubala, R. (2012) Unusual domain architecture of aminoacyl tRNA synthetases and their paralogs from *Leishmania major*. *BMC Genomics* **13,** 621
14. Francklyn, C. (2003) tRNA synthetase paralogs: evolutionary links in the transition from tRNA-dependent amino acid biosynthesis to *de novo* biosynthesis. *Proc. Natl. Acad. Sci. U.S.A.* **100,** 9650–9652
15. Nakamura, M., Yamada, M., Hirota, Y., Sugimoto, K., Oka, A., and Takanami, M. (1981) Nucleotide sequence of the *asnA* gene coding for asparagine synthetase of *E. coli* K-12. *Nucleic Acids Res.* **9,** 4669–4676
16. Sissler, M., Delorme, C., Bond, J., Ehrlich, S. D., Renault, P., and Francklyn, C. (1999) An aminoacyl-tRNA synthetase paralog with a catalytic role in histidine biosynthesis. *Proc. Natl. Acad. Sci. U.S.A.* **96,** 8985–8990
17. Gilreath, M. S., Roy, H., Bullwinkle, T. J., Katz, A., Navarre, W. W., and Ibba, M. (2011) β-Lysine discrimination by lysyl-tRNA synthetase. *FEBS Lett.* **585,** 3284–3288
18. Ambrogelly, A., O'Donoghue, P., Söll, D., and Moses, S. (2010) A bacterial ortholog of class II lysyl-tRNA synthetase activates lysine. *FEBS Lett.* **584,** 3055–3060
19. Yanagisawa, T., Sumida, T., Ishii, R., Takemoto, C., and Yokoyama, S. (2010) A paralog of lysyl-tRNA synthetase aminoacylates a conserved lysine residue in translation elongation factor P. *Nat. Struct. Mol. Biol.* **17,** 1136–1143
20. Roy, H., Zou, S. B., Bullwinkle, T. J., Wolfe, B. S., Gilreath, M. S., Forsyth, C. J., Navarre, W. W., and Ibba, M. (2011) The tRNA synthetase paralog PoxA modifies elongation factor-P with (R)-β-lysine. *Nat. Chem. Biol.* **7,** 667–669
21. Loureiro, I., Faria, J., Clayton, C., Ribeiro, S. M., Roy, N., Santarém, N., Tavares, J., and Cordeiro-da-Silva, A. (2013) Knockdown of asparagine synthetase A renders *Trypanosoma brucei* auxotrophic to asparagine. *PLoS Negl. Trop. Dis.* **7,** e2578
22. Nakatsu, T., Kato, H., and Oda, J. (1998) Crystal structure of asparagine synthetase reveals a close evolutionary relationship to class II aminoacyl-tRNA synthetase. *Nat. Struct. Biol.* **5,** 15–19
23. Thompson, J. D., Higgins, D. G., and Gibson, T. J. (1994) CLUSTAL W: improving the sensitivity of progressive multiple sequence alignment through sequence weighting, position-specific gap penalties and weight matrix choice. *Nucleic Acids Res.* **22,** 4673–4680
24. Pérez-González, J. A., Ruiz, D., Esteban, J. A., and Jiménez, A. (1990) Cloning and characterization of the gene encoding a blasticidin S acetyltransferase from *Streptoverticillum* sp. *Gene* **86,** 129–134
25. Darveau A., Pelletier, A., and Perreault, J. (1995) PCR-mediated synthesis of chimeric molecules. *Methods Neurosci.* **26,** 77–85
26. Kapler, G. M., Coburn, C. M., and Beverley, S. M. (1990) Stable transfection of the human parasite *Leishmania major* delineates a 30-kilobase region sufficient for extrachromosomal replication and expression. *Mol.*

Cell. Biol. **10,** 1084–1094
27. Sambrook, J., Fritsch, E. F., and Maniatis, T. (1989) *Molecular Cloning: A Laboratory Manual*, Cold Spring Harbor Laboratory, Cold Spring Harbor, NY
28. Otwinowski, Z., and Minor, W. (1997) Processing of x-ray diffraction data collected in oscillation mode. *Methods Enzymol.* **276**, 307–326
29. Adams, P. D., Afonine, P. V., Bunkóczi, G., Chen, V. B., Davis, I. W., Echols, N., Headd, J. J., Hung, L. W., Kapral, G. J., Grosse-Kunstleve, R. W., McCoy, A. J., Moriarty, N. W., Oeffner, R., Read, R. J., Richardson, D. C., Richardson, J. S., Terwilliger, T. C., and Zwart, P. H. (2010) PHENIX: a comprehensive Python-based system for macromolecular structure solution. *Acta Crystallogr. D Biol. Crystallogr.* **66,** 213–221
30. Emsley, P., and Cowtan, K. (2004) Coot: model-building tools for molecular graphics. *Acta Crystallogr. D Biol. Crystallogr.* **60,** 2126–2132
31. Pettersen, E. F., Goddard, T. D., Huang, C. C., Couch, G. S., Greenblatt, D. M., Meng, E. C., and Ferrin, T. E. (2004) UCSF Chimera—a visualization system for exploratory research and analysis. *J. Comput. Chem.* **25,** 1605–1612
32. Aurrecoechea, C., Brestelli, J., Brunk, B. P., Fischer, S., Gajria, B., Gao, X., Gingle, A., Grant, G., Harb, O. S., Heiges, M., Innamorato, F., Iodice, J., Kissinger, J. C., Kraemer, E. T., Li, W., Miller, J. A., Nayak, V., Pennington, C., Pinney, D. F., Roos, D. S., Ross, C., Srinivasamoorthy, G., Stoeckert, C. J., Jr., Thibodeau, R., Treatman, C., and Wang, H. (2010) EuPathDB: a portal to eukaryotic pathogen databases. *Nucleic Acids Res.* **38,** D415–D419
33. Chen, F., Mackey, A. J., Stoeckert, C. J., Jr., and Roos, D. S. (2006) OrthoMCL-DB: querying a comprehensive multi-species collection of ortholog groups. *Nucleic Acids Res.* **34,** D363–D368
34. Roy, H., Becker, H. D., Reinbolt, J., and Kern, D. (2003) When contemporary aminoacyl-tRNA synthetases invent their cognate amino acid metabolism. *Proc. Natl. Acad. Sci. U.S.A.* **100,** 9837–9842
35. Burchall, J. J., Reichelt, E. C., and Wolin, M. J. (1964) Purification and properties of the asparagine synthetase of *Streptococcus bovis*. *J. Biol. Chem.* **239,** 1794–1798
36. Chauhan, S. C., and Madhubala, R. (2009) Glyoxalase I gene deletion mutants of *Leishmania donovani* exhibit reduced methylglyoxal detoxification. *PLoS One* **4,** e6805
37. Heinz, E., Williams, T. A., Nakjang, S., Noël, C. J., Swan, D. C., Goldberg, A. V., Harris, S. R., Weinmaier, T., Markert, S., Becher, D., Bernhardt, J., Dagan, T., Hacker, C., Lucocq, J. M., Schweder, T., Rattei, T., Hall, N., Hirt, R. P., and Embley, T. M. (2012) The genome of the obligate intracellular parasite *Trachipleistophora hominis*: new insights into microsporidian genome dynamics and reductive evolution. *PLoS Pathog.* **8,** e1002979
38. Richards, N. G., and Kilberg, M. S. (2006) Asparagine synthetase chemotherapy. *Annu. Rev. Biochem.* **75,** 629–654
39. Pieters, R., Hunger, S. P., Boos, J., Rizzari, C., Silverman, L., Baruchel, A., Goekbuget, N., Schrappe, M., and Pui, C. H. (2011) L-Asparaginase treatment in acute lymphoblastic leukemia: a focus on *Erwinia asparaginase*. *Cancer* **117,** 238–249
40. Koizumi, M., Hiratake, J., Nakatsu, T., Kato, H., and Oda, J. (1999) A potent transition-state analogue inhibitor of *Escherichia coli* asparagine synthetase A. *J. Am. Chem. Soc.* **121,** 5799–5800
41. Boehlein, S. K., Nakatsu, T., Hiratake, J., Thirumoorthy, R., Stewart, J. D., Richards, N. G., and Schuster, S. M. (2001) Characterization of inhibitors acting at the synthetase site of *Escherichia coli* asparagine synthetase B. *Biochemistry* **40,** 11168–11175